Available online at www.sciencedirect.com
ScienceDirect
International Journal of Thermal Sciences 47 (2008) 93–102
International Journal of Thermal Sciences
www.elsevier.com/locate/ijts

Exergetic performance analysis of a solar pond

Mehmet Karakilcik [a], Ibrahim Dincer [b,*]

[a] Department of Physics, Faculty of Sciences and Letters, University of Çukurova, Adana 01330, Turkey
[b] Faculty of Engineering and Applied Science, University of Ontario Institute of Technology (UOIT), 2000 Simcoe Street North, Oshawa, Ontario L1H 7K4, Canada

Received 10 July 2006; received in revised form 27 December 2006; accepted 9 January 2007

Available online 22 February 2007

Abstract

In this paper we present an experimental and theoretical investigation of the exergetic performance of a solar pond (with a surface area of 4 m^2 and a depth of 1.5 m) which was built at Cukurova University in Adana, Turkey. The system was filled with salty water to form three zones (e.g., upper convective, non-convective and heat storage) accordingly. A data acquisition device was used to measure and record the temperatures hourly at various locations in the pond (distributed vertically within and at the bottom of the pond, and horizontally and vertically within the insulated side-walls). An exergy model is developed to study the exergetic performance of the pond and its three zones in terms of exergy efficiencies which are then compared with the corresponding energy efficiencies. The reference environment temperature is specified for exergy analysis as the average representative temperature of each month of the year (for example, it is taken as an average temperature of 28 °C for August). Thus, the highest energy and exergy efficiencies are found for August to be: 4.22% and 3.02% for the upper convective zone, 13.80% and 12.64% for the non-convective zone, and 28.11% and 27.45% for the heat storage zone, respectively.

Keywords: Solar pond; Energy; Exergy; Efficiency; Performance; Thermal system

1. Introduction

Solar radiation constitutes a vast energy source which is abundantly available on all parts of the earth. Solar energy is in many regards one of the best alternatives to non-renewable sources of energy. One way to collect and store solar energy is through the use of solar ponds which can be employed to supply thermal energy for various applications, such as process and space heating, water desalination, refrigeration, drying and power generation. Thermal energy storage has always been the most significant method of energy storage. Solar ponds are a classical application of the thermal energy storage and their performance depends essentially on the storage capacity of the fluid, thermophysical properties of the pond and surroundings conditions [1,2].

Recently, the attention has been paid to the environmentally benign and sustainable energy sources, e.g., solar energy. In this regard, solar ponds appear to be a potential solution for implementation. The literature works can basically be classified into experimental and theoretical ones. Experimental works generally concentrate on design, application, experimental thermal measurements in solar ponds to investigate the thermal efficiencies of various types of solar ponds (e.g., [3–8]). Modeling studies focus on the performance analysis of solar ponds, efficiency determination of the pond zones, alternative operational aspects, etc. (e.g., [9–19]).

To the authors' best knowledge, there have not been experimental and theoretical investigations on exergetic performance analysis of the solar ponds through exergy efficiency. This was in fact the key motivation behind the present work. The present work becomes the first work in the area dealing with the investigation of exergetic performance analysis of the solar pond and comparison with the corresponding energy efficiencies during the months of the year.

* Corresponding author.
E-mail addresses: kkilcik@cu.edu.tr (M. Karakilcik), ibrahim.dincer@uoit.ca (I. Dincer).

1290-0729/$ – see front matter
doi:10.1016/j.ijthermalsci.2007.01.012

Nomenclature

A	surface area	m^2
C	specific heat	$J\,kg^{-1}\,K^{-1}$
E	total solar energy reaching to the pond	J
F	absorbed energy percentage at a region of δ-thickness	
HSZ	heat storage zone	
I	number of the layers, irreversibility	
IB	insulated bottom wall	
ISW	insulated side-walls	
k	thermal conductivity	$J\,m^{-1}\,K^{-1}$
LCZ	lower convective zone	
NCZ	non-convective zone	
Q	heat energy	J
R	thermal resistance of the side-walls	$K\,h\,J^{-1}$
S	thickness	mm
T	temperature	°C
U	heat transfer coefficient between the ambient air and solar pond (hourly basis)	$MJ\,m^{-2}\,K^{-1}\,h^{-1}$
UCZ	upper convective zone	
X	thickness of the inner zones	m

Greek letters

η	energy efficiency	
Ξ	exergy	J
δ	thickness where the long wave solar energy is absorbed	m
β	incident beam entering rate into water	
θ	angle	rad
ρ	density	$kg\,m^{-3}$
Δx	thickness of horizontal layers	mm
ΔS	entropy	$J\,K^{-1}\,mol^{-1}$
$\Delta\Xi$	stored exergy	J
ψ	exergy efficiency	

Subscripts

a	ambient air
b	bottom
g	gained
HSZ	heat storage zone
i	incident
L	length
LCZ	lower convective zone
m	middle; mean
net	net solar irradiation
NCZ	non-convective zone
p	paint
r	reflectance
s	sheet-iron
st	stored
sw	side wall
ti	total input
tl	total loss
UCZ	upper convective zone
w	width
0	reference or reference state
01	painted inner surface area of side wall

2. Experimental apparatus and procedure

Generally solar ponds are thermal storages, which use salt water as the storage fluid, and are essentially divided into three zones as follows:

- The first zone, upper convective zone (UCZ), is the fresh water layer at the top of the pond. This zone is fed with fresh water of a density near to the density of fresh water in the upper part to maintain the cleanliness of the pond and replenish the lost water due to evaporation.
- The second (middle) zone, non-convective zone (NCZ), is composed of salty water layers whose brine density gradually increases towards the lower convective zone (LCZ). The NCZ is the key to the working of a solar pond. It allows an extensive amount of solar radiation to penetrate into the storage zone while inhibiting the propagation of long-wave solar radiation from escaping because water is opaque to infrared radiation.
- The third zone, heat storage zone (HSZ) or LCZ, is composed of salty water with highest density. Considerable part of the solar energy is absorbed and stored by this bottom region. The LCZ has the highest temperature; hence the strongest thermal interaction occurs between this zone and the insulated bottom-wall (IBW) and insulated surrounding side-walls (ISW).

In the experimental work, a solar pond with a surface area of 2 m × 2 m and a depth of 1.5 m was built in Cukurova University in Adana, Turkey (i.e., 35°18′ E longitude, 36°59′ N latitude) and used to measure temperature variations during day and night times at the bottom and side-walls of the pond. The bottom and the side-walls of the pond were plated with the iron-sheets in 0.005 m thickness, and in between with a glass–wool of 50 mm thickness as the insulating layer. Fig. 1 illustrates the inner zones of the solar pond. Inner zones consist of the saline water layers with various densities. The temperature measurements were taken using 16 temperature sensors, which were placed into the inner zones and the insulated walls of the pond. Hence the temperature distribution profiles of these regions at any time were experimentally obtained by a data acquisition system. To measure the temperature distributions of various regions, several temperature sensors were also placed into the inside, starting from the bottom at the heights of 0.05, 0.30, 0.55, 0.70, 0.80, 1.05, 1.35, 1.50 m, from the bottom downwards into the insulated bottom, at 15 and 45 mm and into the side-walls, starting from the bottom at the heights of 0, 0.35, 0.65, 0.75, 1.00, 1.35 m. The data acquisition system was connected

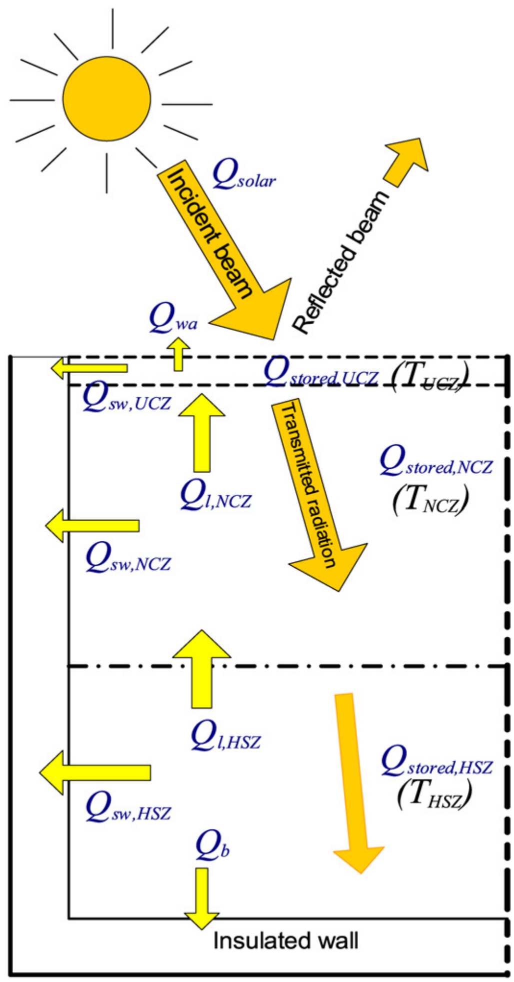

Fig. 1. Schematic representation of the insulated solar pond and energy flows (half-cut view).

to a computer for data recording, monitoring and processing. The inner and wall temperatures of the pond were measured hourly during day and night times. The temperatures at the inner zones and insulated side-wall of the pond were measured by the sensors with a range of −65 to +155 °C, and with a measurement accuracy of ±0.1 °C for the temperature range of 0 to 120 °C. Note that there were no physical compartments or partitions between the zones. The sensors consisted of 1N4148 semi-conductor devices with coaxial cables in different lengths between 17 and 20 m. The solar energy data obtained by using a pyranometer, and hourly average air and daily average insulator temperatures taken from a local meteorological data as input parameters for the modeling part below were used. Further information on experimental system and measurement details (including sensor locations), as well as some thermophysical properties of materials and fluids is available elsewhere [1,2,8].

3. Energy and exergy analyses

An understanding of the relations between exergy and the environment may reveal the underlying fundamental patterns and forces affecting changes in the environment, and help researchers to deal better with environmental damage. Exergy analysis permits many of the shortcomings of energy analysis to be overcome. Exergy analysis acknowledges that, although energy cannot be created or destroyed, it can be degraded in quality, eventually reaching a state in which it is in complete equilibrium with the dead state [2]. It appears to be a potential tool for design, analysis, evaluation, and performance improvement of solar pond systems. Here, Fig. 2 shows each of the zones and the respective exergy flows.

3.1. Energy efficiencies

Here in this section we will briefly summarize the energy efficiencies for each zone of the pond as shown in Fig. 1 for comparing with the corresponding exergy efficiencies which will be obtained later through an exergy analysis. Further information on the detailed energy analysis and efficiency equations development can be available elsewhere [3,4].

- Energy efficiency for the upper convective zone (UCZ):

$$\begin{aligned}\eta_{\mathrm{UCZ}} = 1 - \big\{&A_{01,\mathrm{UCZ}} R_{\mathrm{ps}}(T_{\mathrm{UCZ}} - T_{\mathrm{sw,UCZ}}) \\ &+ U_{\mathrm{wa}} A(T_{\mathrm{UCZ}} - T_{\mathrm{a}})\big\} \Big/ \Big\{\beta E A_{\mathrm{UCZ}}\big[1 - (1-F) \\ &\times h(X_1 - \delta)\big] + \frac{kA}{X_1}(T_{\mathrm{NCZ}} - T_{\mathrm{UCZ}})\Big\}\end{aligned} \tag{1}$$

where T_{a} is the average ambient air temperature, X_1 is the thickness of UCZ; $A_{01,\mathrm{UCZ}}$ is the surface area of the painted metal sheet on the side walls (and taken as $8 \times 0.10 = 0.8\ \mathrm{m}^2$); δ is the thickness of the layer in UCZ absorbing the long-wave solar incident radiation; F is energy ratio by percent absorbed at a region of δ-thickness, E is the total solar radiation incident coming on the pond surface, A is the upper surface area of the pond; k is the thermal conductivity of the layers in UCZ; R_{ps} is the thermal resistance of the painted metal sheet surrounding the first layer, respectively as $R_{\mathrm{ps}} = \frac{k_{\mathrm{p}} k_{\mathrm{s}}}{S_{\mathrm{p}} k_{\mathrm{s}} + S_{\mathrm{s}} k_{\mathrm{p}}}$ (here k_{p} and k_{s} are thermal conductivities of the paint and iron-sheet, and S_{p} and S_{s} are the corresponding thicknesses).

Also β is the fraction of the incident solar radiation that enters the pond, and is written using an expression by [10]:

$$\beta = 1 - 0.6\left[\frac{\sin(\theta_{\mathrm{i}} - \theta_{\mathrm{r}})}{\sin(\theta_{\mathrm{i}} + \theta_{\mathrm{r}})}\right]^2 - 0.4\left[\frac{\tan(\theta_{\mathrm{i}} - \theta_{\mathrm{r}})}{\tan(\theta_{\mathrm{i}} + \theta_{\mathrm{r}})}\right]^2$$

(here θ_{i} and θ_{r} are the angles of incident and reflected solar radiation).

The ratio of the solar energy reaching the bottom of layer I to the total solar radiation incident on to the surface of the pond (h) is given by Bryant and Colbeck [20] as

$$h_I = 0.727 - 0.056 \ln\left[\frac{(X_1 - \delta)}{\cos\theta_{\mathrm{r}}}\right]$$

which should be h_1 in Eq. (1), and h_2 and h_3 in Eqs. (2) and (3), respectively.

Also, A_{UCZ} is the net upper surface area of UCZ, as the effective area that receives incident solar radiation and is defined as $A_{\mathrm{UCZ}} = L_{\mathrm{w}}[L_{\mathrm{L}} - (\delta + (I-1)\Delta x)\tan\theta_{\mathrm{r}}]$ (here θ_{r}

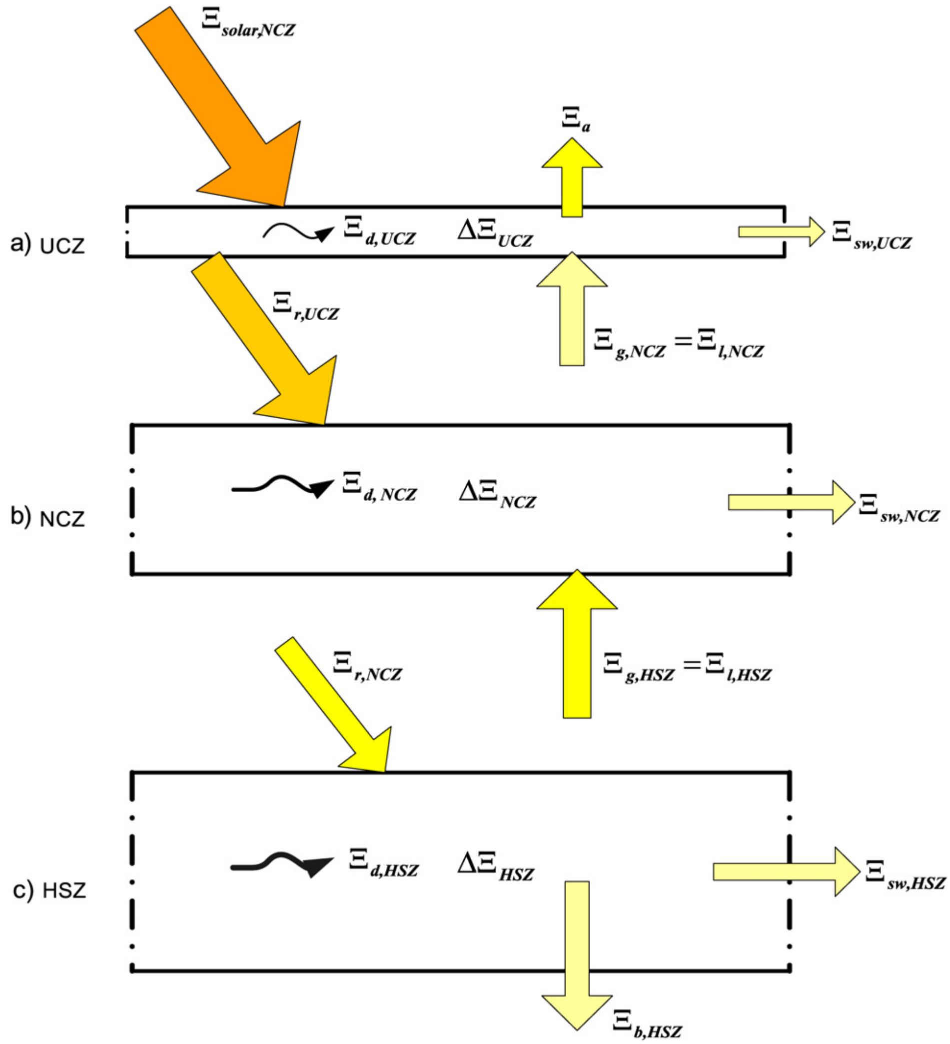

Fig. 2. Exergy flows in the inner zones of the solar pond as (a) upper convective zone (UCZ), (b) non-convective zone (NCZ), (c) heat storage zone (HSZ).

the angle of the reflected incidence, Δx is the thickness of each layer in UCZ and taken as 0.05 m in the calculations, and L_w and L_L are the width and length of the pond).

- Energy efficiency for the non-convective zone (NCZ):

$$\eta_{NCZ} = 1 - \left\{ \frac{kA}{\Delta X}(T_{NCZ} - T_{UCZ}) + A_{01,NCZ} R_{ps}(T_{NCZ} - T_{sw,UCZ}) \right\} \Big/ \left\{ \beta E A_{NCZ}\big[(1-F)\big[h(X_1-\delta) - h(X_1-\delta+\Delta x)\big]\big] + \frac{kA}{\Delta X}(T_{HSZ} - T_{NCZ}) \right\} \quad (2)$$

where $A_{01,NCZ}$ is the surface area of the painted metal sheet on the side walls surrounding of NCZ (and taken as $8 \times 0.60 = 4.8$ m^2); F is the fraction of the incident solar radiation absorbed by the pond's upper layer; and A_{NCZ} is the net upper surface area of NCZ $A_{NCZ} = L_w[L_L - (X_1 + (I-1)\Delta x)\tan\theta_r]$ (here I varies from 2 to 14, respectively).

- Energy efficiency for the heat storage zone (HSZ):

$$\eta_{HSZ} = 1 - \left\{ A R_{ps}(T_{HSZ} - T_b) + \frac{kA}{\Delta X_{HSZ}}(T_{HSZ} - T_{NCZ}) + A_{01,HSZ} R_{ps}(T_{HSZ} - T_{sw,UCZ}) \right\} \Big/ \left\{ \beta E A_{HSZ}\big[(1-F)h(X_3-\delta)\big] \right\} \quad (3)$$

where $A_{01,HSZ}$ is the surface area of the painted metal sheet on the side walls surrounding of HSZ (and taken as $8 \times 0.80 = 6.4$ m^2); T_b is the bottom temperature; $\Delta X_{HSZ} = (X_3 - X_2)$ is the thickness of the HSZ of the pond. Note $A_{HSZ,I} = A_{NCZ,I}$ with I, varying from 15 to 30, respectively. Note that the depth of the pond is divided into 30 nodes where the temperature sensors were placed for measurements.

3.2. Exergy analysis

Here we present a comprehensive exergy analysis of each zone with the exergetic efficiency. The exergy flows are well outlined in Fig. 2.

3.2.1. Exergy analysis for UCZ

As shown in Fig. 2(a), the exergy flows in UCZ can be illustrated. We first write the exergy balance equation for UCZ as

$$\Xi_{\text{solar}} + \Xi_{\text{g,NCZ}} = \Xi_{\text{r,UCZ}} + \Xi_{\text{d,UCZ}} + \Xi_{\text{a}} + \Xi_{\text{sw,UCZ}} \tag{4}$$

where Ξ_{solar} is the exergy of solar radiation reaching UCZ surface, $\Xi_{\text{g,NCZ}}$ is the exergy gained from NCZ, $\Xi_{\text{r,UCZ}}$ is the recovered exergy of UCZ for NCZ, $\Xi_{\text{d,UCZ}}$ is the exergy destruction in UCZ, $\Xi_{\text{a,UCZ}}$ is the exergy loss from UCZ to the ambient air and $\Xi_{\text{sw,UCZ}}$ is the exergy loss through side walls.

Here $\Xi_{\text{r,UCZ}}$ can be written according to Eq. (4) as

$$\begin{aligned}\Xi_{\text{r,UCZ}} &= \Xi_{\text{ti}} - \Xi_{\text{tl}} \\ &= (\Xi_{\text{solar}} + \Xi_{\text{g,NCZ}}) - (\Xi_{\text{d,UCZ}} + \Xi_{a} + \Xi_{\text{sw,UCZ}})\end{aligned} \tag{5}$$

where Ξ_{tl} is the total exergy losses, including exergy destruction. And Ξ_{ti} is the total exergy input to UCZ.

Here the exergy of solar radiation can be expressed (as modified from Petela [21]):

$$\Xi_{\text{solar}} = E_{\text{net}}\left[1 - \frac{4T_0}{3T} + \frac{1}{3}\left(\frac{T_0}{T}\right)^4\right]A_{\text{UCZ}} \tag{6}$$

and the exergy gained from NCZ is

$$\Xi_{\text{g,NCZ}} = m_{\text{NCZ}}C_{\text{p,NCZ}}\left[(T_{\text{m,NCZ}} - T_{\text{UCZ}}) - T_0\left(\ln\frac{T_{\text{m,NCZ}}}{T_{\text{UCZ}}}\right)\right] \tag{7}$$

where E_{net} is the net incident solar radiation reaching UCZ surface; A_{UCZ} is the net surface area of UCZ; and T is the sun's surface temperature taken as 6000 K [21]; T_0 is the reference or reference state temperature; T_m is the mean temperature; $m_{\text{NCZ}} = \rho_{\text{NCZ}}V_{\text{NCZ}}$ is the mass of salty water in NCZ; ρ_{NCZ} is the averaged density as given earlier [3]; and V_{NCZ} is the volume of the salty water in NCZ as $V_{\text{NCZ}} = 2.4\ \text{m}^3$.

The exergy destruction in UCZ is basically written as

$$\Xi_{\text{d,UCZ}} = T_0(\Delta S_{\text{net}}) \tag{8}$$

where ΔS_{net} is the net entropy change of UCZ which is defined $\Delta S_{\text{net}} = \Delta S_{\text{sys}} + \Delta S_{\text{surr}}$. After substituting each of the entropy change term, Eq. (8) becomes

$$\Xi_{\text{d,UCZ}} = T_0\left[m_{\text{UCZ}}C_{\text{p,UCZ}}\ln\frac{T_{\text{UCZ}}}{T_0} - \left(\frac{Q_{\text{wa}}}{T_{\text{UCZ}}} + \frac{Q_{\text{sw,UCZ}}}{T_0}\right) + \left(\frac{Q_{\text{g,NCZ}}}{T_{\text{NCZ}}} + \frac{Q_{\text{sw,UCZ}}}{T_0}\right)\right] \tag{9}$$

In addition, we write the exergy losses to the ambient air and through side walls in the following manner:

$$\Xi_{\text{a,UCZ}} = m_{\text{UCZ}}C_{\text{p,UCZ}}\left[(T_{\text{UCZ}} - T_{\text{a}}) - T_0\left(\ln\frac{T_{\text{UCZ}}}{T_{\text{a}}}\right)\right] \tag{10}$$

and

$$\Xi_{\text{sw,UCZ}} = m_{\text{UCZ}}C_{\text{p,sw}}\left[(T_{\text{UCZ}} - T_{\text{sw,UCZ}}) - T_0\left(\ln\frac{T_{\text{UCZ}}}{T_{\text{sw,UCZ}}}\right)\right] \tag{11}$$

where, $m_{\text{UCZ}} = \rho_{\text{UCZ}}V_{\text{UCZ}}$ is the mass of salty water in UCZ; ρ_{UCZ} is the averaged density as given earlier [3]; and V_{UCZ} is the volume of the salty water in UCZ as $V_{\text{UCZ}} = 0.4\ \text{m}^3$. $C_{\text{p,UCZ}}$ and $C_{\text{p,sw}}$ are the specific heats of UCZ and insulating material; T_{a} and T_0 are the ambient temperature and the reference environment temperature; T_{UCZ}, $T_{\text{sw,UCZ}}$ and $T_{\text{m,NCZ}}$ denote the average temperatures of UCZ, side wall and nonconvective zone, respectively.

We can now define the exergy efficiency for UCZ as the ratio of the exergy recovered from UCZ to the total exergy input to UCZ:

$$\psi_{\text{UCZ}} = \frac{\Xi_{\text{r,UCZ}}}{\Xi_{\text{ti}}} = 1 - \frac{\Xi_{\text{d,UCZ}} + \Xi_{\text{a}} + \Xi_{\text{sw,UCZ}}}{\Xi_{\text{solar}} + \Xi_{\text{g,NCZ}}} \tag{12}$$

3.2.2. Exergy analysis for the NCZ

Fig. 2(b) shows the exergy flows in NCZ, and the exergy balance equation can be written as

$$\Xi_{\text{r,UCZ}} + \Xi_{\text{g,HSZ}} = \Xi_{\text{r,NCZ}} + \Xi_{\text{d,NCZ}} + \Xi_{\text{l,NCZ}} + \Xi_{\text{sw,NCZ}} \tag{13}$$

where $\Xi_{\text{r,UCZ}}$ is the exergy recovered from UCZ; $\Xi_{\text{g,HSZ}}$ is the exergy gained from HSZ, $\Xi_{\text{r,NCZ}}$ is the recovered exergy of NCZ for HSZ, $\Xi_{\text{d,NCZ}}$ is the exergy destruction in NCZ, $\Xi_{\text{l,NCZ}}$ is the exergy loss from NCZ to UCZ and equivalent to $\Xi_{\text{g,NCZ}}$, and $\Xi_{\text{sw,NCZ}}$ is the exergy loss through side walls.

Table 1
Average reference environment temperatures and average exergy contents of each zone

Months	January	February	March	April	May	July	August	September	October	November	December
Reference tem. (°C)	10.0	11.0	14.2	17.6	22.0	28.0	28.0	26.0	21.0	16.0	11.0
Exergy input (UCZ) (MJ)	417.40	644.32	1160.85	1700.20	1976.24	2167.89	1982.47	1740.41	1299.94	782.72	506.14
Exergy recovered (MJ)	329.42	510.50	920.75	1347.54	1552.53	1681.57	1524.70	1344.78	1004.95	614.02	393.03
Exergy input (NCZ) (MJ)	335.05	516.70	930.67	1363.33	1588.13	1747.54	1601.34	1404.25	1048.74	629.23	407.89
Exergy recovered (MJ)	187.77	290.90	524.82	768.09	884.94	958.49	869.08	766.52	572.82	349.99	224.03
Exergy input (HCZ) (MJ)	187.77	290.90	524.82	768.09	884.94	958.49	869.08	766.52	572.82	349.99	224.03
Exergy stored (MJ)	17.12	27.19	53.15	89.27	140.79	204.40	218.00	181.39	133.28	57.03	27.92

Here $\Xi_{r,NCZ}$ can be extracted from Eq. (13) as

$$\Xi_{r,NCZ} = \Xi_{ti,NCZ} - \Xi_{tl,NCZ} = (\Xi_{r,UCZ} + \Xi_{g,HSZ}) - (\Xi_{d,NCZ} + \Xi_{l,NCZ} + \Xi_{sw,NCZ}) \tag{14}$$

with

$$\Xi_{g,HSZ} = m_{HSZ} C_{p,HSZ}\left[(T_{HSZ} - T_{NCZ}) - T_0\left(\ln\frac{T_{HSZ}}{T_{NCZ}}\right)\right] \tag{15}$$

where $m_{HSZ} = \rho_{HSZ} V_{HSZ}$ is the mass of salty water in HSZ; ρ_{HSZ} is the averaged density as given earlier [3]; and V_{HSZ} is the volume of salty water in HSZ as $V_{HSZ} = 3.2\ \text{m}^3$.

The exergy destruction in NCZ is then written as

$$\Xi_{d,NCZ} = T_0(\Delta S_{net,NCZ}) \tag{16}$$

where $\Delta S_{net,NCZ}$ is the net entropy change of NCZ which is $\Delta S_{net,NCZ} = \Delta S_{sys} + \Delta S_{surr}$.

Then, the exergy losses, including exergy destruction within NCZ, can be derived as follows:

$$\Xi_{d,NCZ} = T_0\left[m_{NCZ} C_{p,NCZ} \ln\frac{T_{m,NCZ}}{T_0} - \left(\frac{Q_{g,NCZ}}{T_{m,NCZ}} + \frac{Q_{sw,NCZ}}{T_0}\right) + \left(\frac{Q_{g,HSZ}}{T_{m,NCZ}} + \frac{Q_{sw,NCZ}}{T_0}\right)\right] \tag{17}$$

$$\Xi_{l,NCZ} = m_{NCZ} C_{p,NCZ}\left[(T_{m,NCZ} - T_{UCZ}) - T_0\left(\ln\frac{T_{m,NCZ}}{T_{UCZ}}\right)\right] \tag{18}$$

$$\Xi_{sw,NCZ} = m_{NCZ} C_{p,sw}\left[(T_{m,NCZ} - T_{sw,NCZ}) - T_0\left(\ln\frac{T_{m,NCZ}}{T_{sw,NCZ}}\right)\right] \tag{19}$$

where $C_{p,NCZ}$ is the specific heat of NCZ; T_{HSZ} is the average temperature of HSZ.

We can now define the exergy efficiency for the NCZ as the ratio of the exergy recovered from NCZ to the total exergy input to NCZ:

$$\psi_{NCZ} = \frac{\Xi_{r,NCZ}}{\Xi_{ti}} = 1 - \frac{\Xi_{d,NCZ} + \Xi_{l,NCZ} + \Xi_{sw,NCZ}}{\Xi_{r,UCZ} + \Xi_{g,HSZ}} \tag{20}$$

3.2.3. Exergy analysis for HSZ

The exergy flows in HSZ are clearly shown in Fig. 2(c) and the exergy balance equation in this regard results in

$$\Xi_{r,NCZ} - (\Xi_{d,HSZ} + \Xi_{l,HSZ} + \Xi_{sw,HSZ} + \Xi_{b,HSZ}) = \Delta\Xi_{st} \tag{21}$$

where $\Xi_{r,NCZ}$ is the recovered exergy from NCZ for HSZ, $\Xi_{d,HSZ}$ is the exergy destruction in HSZ, $\Xi_{l,HSZ}$ is the exergy loss from HSZ to NCZ, $\Xi_{sw,HSZ}$ is the exergy loss through side walls. $\Xi_{b,HSZ}$ is the exergy loss through bottom wall and also, $\Delta\Xi_{st}$ is the exergy stored in HSZ.

Here $\Xi_{d,HSZ}$ is the exergy destruction in HSZ which can be written as

$$\Xi_{d,HSZ} = T_0(\Delta S_{net,HSZ}) \tag{22}$$

where $\Delta S_{net,HSZ}$ is the net entropy change of HSZ as $\Delta S_{net,HSZ} = \Delta S_{sys} + \Delta S_{surr}$.

The exergy losses, including exergy destruction within NCZ, can be derived as follows:

$$\Xi_{d,HSZ} = T_0\left[m_{HSZ} C_{p,HSZ} \ln\frac{T_{HSZ}}{T_0} - \left(\frac{Q_{g,HSZ}}{T_{HSZ}} + \frac{Q_{sw,HSZ}}{T_0}\right) + \left(\frac{Q_b}{T_0}\right)\right] \tag{23}$$

$$\Xi_{l,HSZ} = m_{HSZ} C_{p,HSZ}\left[(T_{HSZ} - T_{m,NCZ}) - T_0\left(\ln\frac{T_{HSZ}}{T_{m,NCZ}}\right)\right] \tag{24}$$

where $C_{p,HSZ}$ is the specific heat of salty water in HSZ.

$$\Xi_{sw,HSZ} = m_{HSZ} C_{p,sw}\left[(T_{HSZ} - T_{sw,HSZ}) - T_0\left(\ln\frac{T_{HSZ}}{T_{sw,HSZ}}\right)\right] \tag{25}$$

Note $\Xi_{b,HSZ} = \Xi_{sw,HSZ}$, due to the fact that both side wall and bottom layer have the same insulating materials and are surrounded by the ambient air.

We can now define the exergy efficiency for HSZ as the ratio of the exergy stored in HSZ to the total exergy input to HSZ which is essentially the exergy recovered from NCZ:

$$\psi_{HSZ} = \frac{\Delta\Xi_{st}}{\Xi_{r,NCZ}} = 1 - \frac{\{\Xi_{d,HSZ} + \Xi_{l,HSZ} + \Xi_{sw,HSZ} + \Xi_{b,HSZ}\}}{\Xi_{r,NCZ}} \tag{26}$$

It is important to highlight that exergy is a potential to help achieve better efficiency and effectiveness of the process/system due to some key benefits, such as:

- furthering the goal of more efficient energy resource utilization,
- enabling locations, types and true magnitudes of wastes and losses to be determined, and
- revealing whether or not and how much it is possible to design more efficient energy systems by reducing the inefficiencies in the process/system.

4. Results and discussion

Here we now present the results of the model calculations for both energy and exergy efficiencies of each zone in the experimental solar pond as upper convective zone (UCZ), non-convective zone (NCZ) and heat storage zone (HSZ) and compare these results to show how exergy is crucial for determining true magnitudes of the losses taking place in each zone and finding the true values of each zone.

It has been demonstrated that the stability of salt density distribution in a solar pond is of great significance as shown in Fig. 3. It is now well known that any reduction in salt gradient region decreases the pond's ability to store heat energy and hence increases the molecular diffusion flow. The primary reason for differences during different months is likely the higher

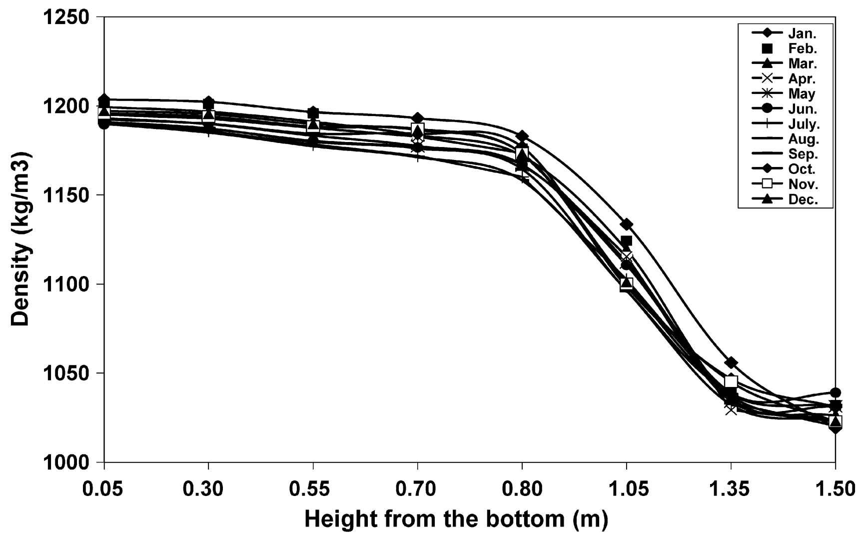

Fig. 3. The variations of the salt density in the inner zones of the solar pond.

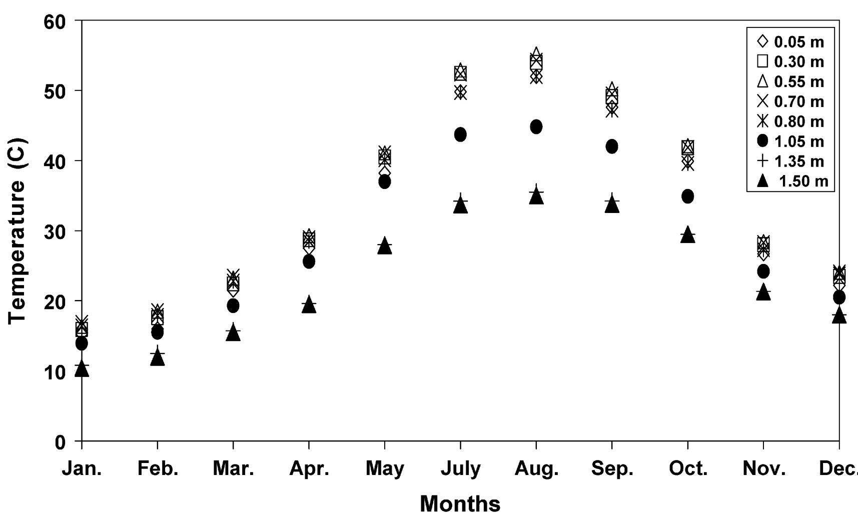

Fig. 4. Experimental zone temperature distributions in the inner zones of the solar pond.

temperatures in summer. This change is mainly attributable to the thermo-physical property of the salty water, heat losses from the pond to the air, and the absorption and reflection of incident solar radiation on the surface. The reason for the fluctuations in the saline density in UCZ and NCZ was the increase in saline density of these zones due to the evaporation of the water at the upper region. These changes can be reduced by continuously adding fresh water to the top of the pond. Due to the non-availability of one of the salt gradient protection systems for cleaning purposes for a month, significant changes occurred in the UCZ and NCZ. In fact, Fig. 3 shows the averaged experimental density variations of salty water versus the height of the pond from the bottom in twelve months at different dates. There were little differences between these density distributions measured in January, April and July, due to the temperature changes and some evaporation of salty water from the pond. As expected, increasing temperature decreased the density more in the summer months. Generally, these changes could be eliminated by continuous adding of fresh water to the top of the pond. Due to the cancellation of one of the salt gradient protection systems for cleaning purposes for a month, some changes occurred in the non-convective region and upper convective region.

The zone temperatures of the pond were measured throughout the months and averaged to find the monthly average temperature values at the respective points. It is clear that the zone temperatures vary with month of the year, depending on the environment temperature and incoming solar incidence. The temperatures of the zones generally increase with incident solar energy per unit area of surface. There are heat losses from each zone and this is the largest in the storage zone which affects the storage performance directly and drastically. In order to improve the performance and increase the efficiency, we should minimize the losses appropriately. Regarding the experimental temperature distributions in Fig. 4 for the zones, the temperature of the UCZ is observed to be a maximum of 35.0 °C in August, a minimum of 10.4 °C in January, and 27.9 °C in May. Similarly, the temperature of the NCZ is observed to be a max-

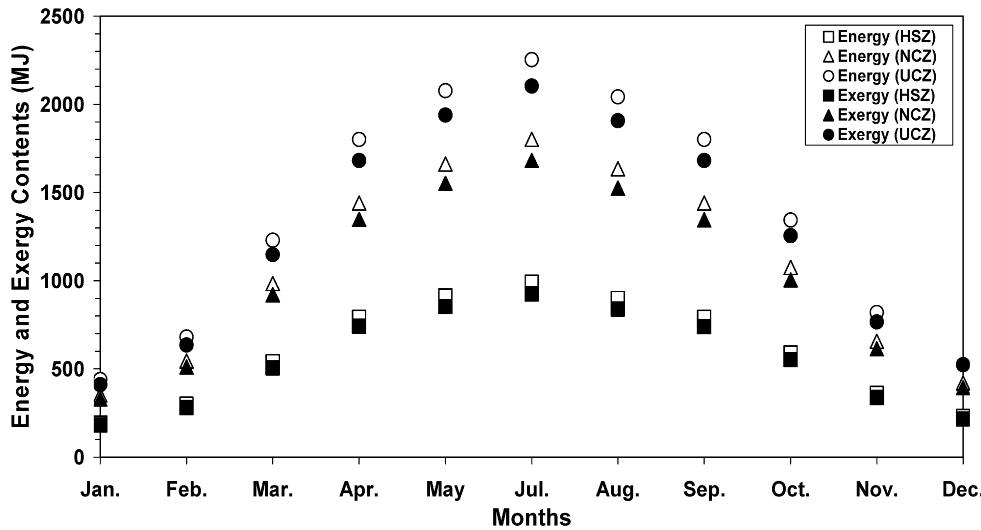

Fig. 5. Energy and exergy content distributions of the solar pond zones.

imum of 44.8 °C in August, a minimum of 13.9 °C in January, and 37.9 °C in May, while the temperature of the HSZ is observed to be a maximum of 55.20 °C in August, a minimum of 16.91 °C in January, and 41.10 °C in May. The exergy content distributions in the zones are the calculated using the reference environment temperatures taken as the monthly average temperatures as listed in Table 1.

Fig. 5 shows both averaged energy and exergy content variations of the three zones (UCZ, NCZ and HSZ) of the pond versus months of the year, based on the experimental data. For the first layer (UCZ) it is the solar radiation reaching its surface; for NCZ it is the one recovered from UCZ; and for HSZ it is the one recovered from NCZ. As seen here in the figure, the exergy contents are less than the corresponding energy contents due to the fact that energy is conserved, but not exergy. So, some exergy is destructed in the each zone in addition to the exergy losses to the surrounding air. As seen in Fig. 5, the lowest exergy contents appear in January and the highest ones in July. Of course, the surroundings temperature plays a key role since the energy and exergy losses are rejected to the ambient air. It is important to mention that the shape of the energy and exergy content distributions follow the solar irradiation profile closely.

Fig. 6 shows the variations of exergy input, exergy recovered, and exergy destruction and losses taking place in the UCZ for 11 months of the year, except for the month of June where the measurements were not taken due to maintenance of data acquisition system. As apparent here, the exergy inputs are equivalent to the summation of exergy recovered and exergy destruction and losses. It is assumed that there is no accumulation in this zone, due to fact that through calculations we obtained that it is less than 1%. As the figure shows, the exergy input becomes highest in July due to the highest incoming solar irradiation, and the other exergy items appear to be proportional to the input. The exergy recovered in this zone goes to the NCZ and the maximum and minimum exergy recovered are 1681.57 MJ in July and 392.42 MJ in January, respectively. The trend of the bars is consistent with the changes in Fig. 5.

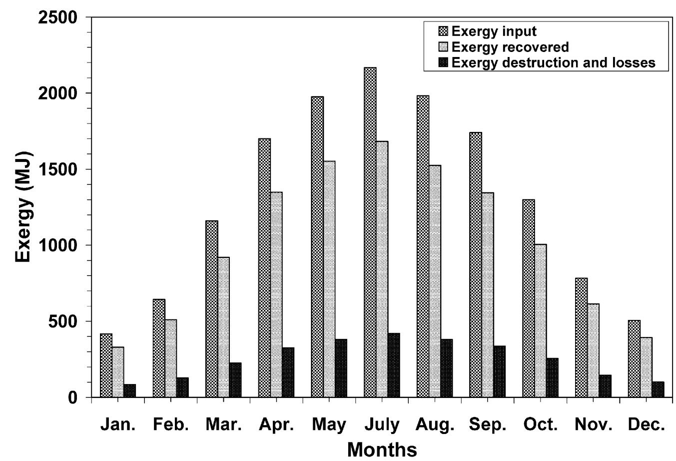

Fig. 6. Exergy distributions in the upper convective zone of the solar pond.

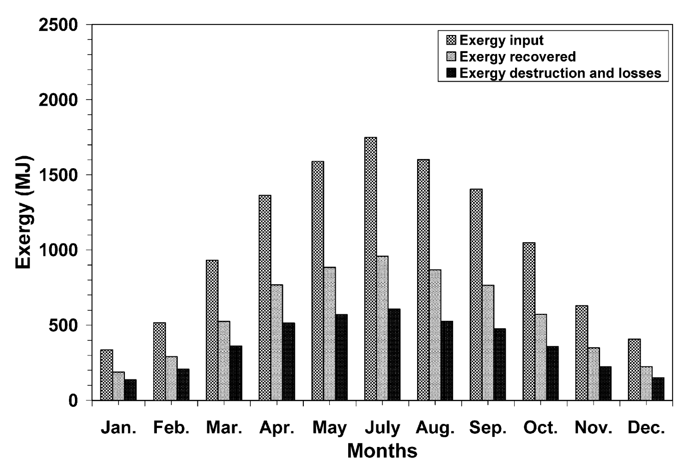

Fig. 7. Exergy distributions in the non-convective zone of the solar pond.

Fig. 7 shows the variations of exergy input, exergy recovered, and exergy destruction and losses taking place in the NCZ during the eleven months of the year. It is obvious that the exergy inputs are equivalent to the summation of exergy recovered and exergy destruction and losses. Here in this zone, it is assumed that there is no accumulation, due to fact that through calculations we obtained that it is less than 1%. It is also shown that the exergy input becomes highest in July due to the highest incoming solar irradiation, and the other exergy items appear to be proportional to the input. The exergy recovered in this zone goes to the NCZ and the maximum and minimum exergy recovered are 958.49 MJ in July and 187.77 MJ in January, respectively. The exergy inputs to and recovered from this zone are listed in Table 1.

As consistent with what Jaefarzadeh [8] stated, salt-gradient solar ponds promise to be one of the relatively simple sources of energy collection and thermal storage with a cheap cost per unit area. In such ponds, saline is stored in three layers increasing in density. The surface layer is homogeneous and convective, where the density of saline is close to fresh water. In the middle layer saline density increases in depth, thereby natural convection is stopped. In this layer, mass or thermal energy is transported only by molecular diffusion that is a very low process. The lowest layer is dense and convective, and has a relatively uniform density close to saline saturation. That part of solar irradiation which transmits to this layer increases its temperature. The heat stored there can only be transferred through the middle layer by conduction. Therefore, the middle non-convective layer acts as an insulator. The thermal energy collected in the lowest layer may be utilized later.

It is also important to mention that in practice the convection in solar ponds is inhibited by raising the viscosity of the pond by adding gelling agents, for example, a polyethyleneoxide adduct of a hydrophobic residue. Convection is further inhibited by dividing the pond into cells such that the Rayleigh number of the fluid within the cell structure is less than the critical Rayleigh number at which convection may occur. The dividers may be translucent or transparent generally horizontal sheets or generally vertical sheets, forming matrices which are rectangular, hexagonal or triangular in horizontal cross-sections. Alternatively, the gelled fluid medium of the solar pond may be bagged in translucent elongated bags which when arranged in the pond have their shortest dimension less than that which will support convection.

Fig. 8 exhibits in a bar chart the distributions of exergy input, exergy stored, and exergy destruction and losses taking place in the HSZ during the eleven months of the year (except for June). In this zone, we have exergy stored, instead of exergy recovered since the HSZ is the last zone, due to fact that this is why we run solar ponds to do daily and/or seasonal (or long-term) storage. It is clear that the exergy inputs are equivalent to the summation of exergy recovered and exergy destruction and losses for the UCZ and NCZ, respectively. The exergy stored becomes smallest compared to the exergy inputs and exergy destruction and losses in the HSZ, and appears to be maximum in July as 743.10 MJ and minimum in January as 169.68 MJ, respectively. The values for each month are seen in Fig. 8. It is important to mention that exergy destruction in the HSZ is caused by entropy generation directly which is a function of both entropy change within the system and entropy change in the surroundings due to the heat rejection. In both cases, the driving force for exergy destruction (or entropy generation) is the differences/changes between system and surrounding temperatures and pressures. In most cases, the pressure difference is negligibly small while the temperature difference is considerable.

Fig. 9 shows a comparison of both energy and exergy efficiencies and their variations based on the experimental data measured during the eleven months of the year (except for June). As seen in the figure, the differences between energy and exergy efficiencies are small in cooler months, and largest from May to October. As expected, the efficiencies for the HSZ are higher than the corresponding UCZ and NCZ efficiencies.

As a result, the inner zones of the pond store more exergy in July than in January due to the considerable temperature differences between the zones. The exergy destruction and losses significantly affect the performance of the pond and should be minimized to increase the system efficiency.

Furthermore, the advantages of exergy analysis of such systems for design, analysis and performance improvement purposes are that it helps achieve the goal of more efficient energy resource utilization, enabling locations, types and true magnitudes of wastes and losses to be determined, and revealing whether or not and how much it is possible to design more

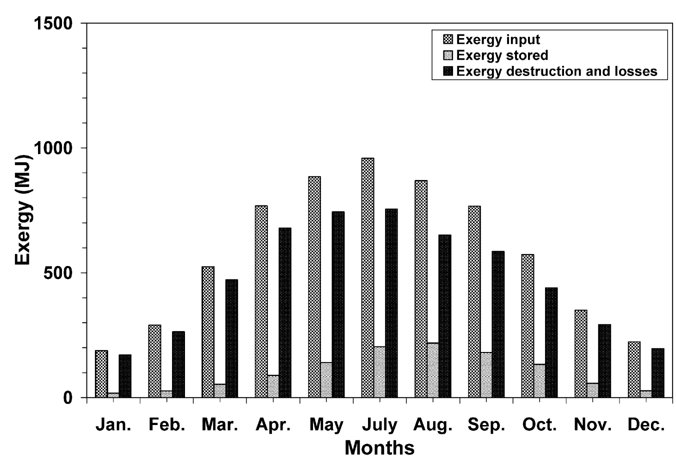

Fig. 8. Exergy distributions and exergy stored in the heat storage zone of the solar pond.

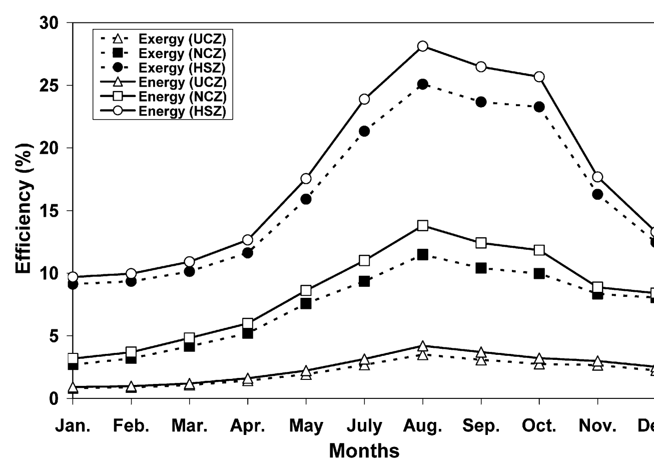

Fig. 9. Variations of the energy and exergy efficiencies of the solar pond zones.

efficient energy systems by reducing the inefficiencies in the process/system.

5. Conclusions

In this paper we have studied both energetic and exergetic performances of a solar pond through efficiency analysis. Exergy efficiencies were developed for each zone of the solar pond (upper convective, non-convective and heat storage zones) through exergy balance equations. The exergy efficiencies determined for each zone using the experimental data are compared with the corresponding energy efficiencies. As expected, the exergy efficiencies appear to be little less than the energy efficiencies for each zone of the pond due to the small magnitudes of exergy destructions in the zones and losses to the surroundings. It is important to determine the true magnitudes of these destructions and losses and minimize these for performance improvement of the pond.

Acknowledgements

The authors acknowledge the support provided by Cukurova University in Turkey, and the Natural Sciences and Engineering Research Council of Canada in Canada.

References

[1] I. Dincer, M.A. Rosen, A worldwide perspective on energy, environment and sustainable development, Int. J. Energy Res. 22 (15) (December 1998) 1305–1321.
[2] I. Dincer, M.A. Rosen, Thermal Energy Storage: Systems and Applications, John Wiley and Sons, New York, USA, 2003.
[3] M. Karakilcik, I. Dincer, M.A. Rosen, Performance investigation of a solar pond, Appl. Thermal Engrg. 26 (2006) 727–735.
[4] M. Karakilcik, K. Kıymaç, I. Dincer, Experimental and theoretical distributions in a solar pond, Int. J. Heat Mass Transfer 49 (2006) 825–835.
[5] M. Karakilcik, Determination of the performance of an insulated prototype solar pond, Ph.D. Thesis, University of Cukurova, Adana, Turkey, 1998 (in Turkish).
[6] R.S. Beniwal, R. Singh, N.S. Saxena, R.C. Bhandari, Thermal behaviour of salt gradient solar ponds, J. Phys. D: Appl. Phys. 20 (1987) 1067–1071.
[7] K. Kanayama, H. Inaba, H. Baba, T. Fukuda, Experimental analysis of particle-scale solar pond stabilized with salt gradient, Solar Energy 46 (1991) 353–359.
[8] M.R. Jaefarzadeh, Thermal behavior of a small salinity-gradient solar pond with wall shading effect, Solar Energy 77 (2004) 281–290.
[9] M.A. Hassab, O.A. El-Masry, Effects on solar-energy collection in small solar ponds, Appl. Energy 38 (1983) 81–94.
[10] M.N.A. Hawlader, The influence of the extinction coefficient on the effectiveness of solar ponds, Solar Energy 25 (1980) 461–464.
[11] H. Kurt, F. Halici, A. Korhan Binark, Solar pond conception—experimental and theoretical studies, Energy Conversion Management 41 (9) (2000) 939–951.
[12] A.S. Mehta, N. Pathak, B.M. Shah, S.D. Gomkale, Performance analysis of a bittern-based solar pond, Solar Energy 240 (1988) 469–475.
[13] K.A. Meyer, A numerical model for describing the layer behaviour in salt-gradient solar ponds, Trans. ASME J. Solar Energy Engrg. 105 (1983) 341–347.
[14] T.A. Newell, R.G. Cowie, J.M. Upper, M.K. Smith, G.L. Cler, Construction and operation activities at the University of Illinois salt gradient solar pond, Solar Energy 45 (4) (1990) 231–239.
[15] C.E. Nielsen, Experience with a prototype solar pond space heating, Solar Energy 5 (1976) 169–182.
[16] M. Ouni, A. Guizani, H. Lu, A. Belghith, Simulation of the control of a salt gradient solar pond in the south of Tunisia, Solar Energy 75 (2) (2003) 95–101.
[17] M.R.I. Ramadan, A.A. El-Sebaii, S. Aboul-Enein, A.M. Khallaf, Experimental testing of a shallow solar pond with continuous heat extraction, Energy & Buildings 36 (2004) 955–964.
[18] A. Sozen, Effect of irreversibilities on performance of an absorption heat transformer used to increase solar pond's temperature, Renewable Energy 29 (2003) 501–515.
[19] H. Weinberger, The physics of solar pond, Solar Energy 8 (1964) 45–56.
[20] H.C. Bryant, I. Colbeck, A solar pond for London, Solar Energy 19 (1977) 321.
[21] R. Petala, Exergy of undiluted thermal radiations, Solar Energy 74 (2003) 469–488.